Radiation Effects in Image Guide Structures

Iliyana I. Arestova and Valda P. Levcheva

Abstract — **The coupled image guide (IG) structures represent a possible solution for components at millimeter wavelengths. The difficulties in the design and optimization of such type of devices are due particularly to the processes of reflection and radiation at the existing open ends of the IG. In an attempt to clear up the processes taking place, we have examined both experimentally and numerically the open ended IG structure.**

Keywords — **image guide (IG), millimeter wavelengths, radiation.**

I. INTRODUCTION

THE image guide (IG) has been considered for the component applications at millimeter wave lengths by many investigators [1], [2]. The IG structures proposed usually contain coupled IGs. Both reciprocal and nonreciprocal IG structures have been investigated, the latter usually containing magnetized ferrites. One of the configurations [3], [4] includes a coupling between two IGs – primary and secondary (Fig. 1a). Because of the finite length of the secondary IG the processes of reflection and radiation arise in the structure that should be considered in the design procedure of the components.

Here we have examined the simplest open ended IG structure (Fig. 1b). First we have used electric probes to measure experimentally the distribution of the electric field components. After that, we have used the finite element method (FEM) to simulate the same IG structure numerically.

II. EXPERIMENTAL INVESTIGATION

The electric probes (Fig. 2) contain a section of a 50 Ohm semi-rigid coaxial cable, which has its outer conductor removed at the length of about a quarter of a wavelength. The electric probe for the E_y component contains a straight vertical section of the inner conductor, while the electric probe for E_x and E_z – a 90º bend section. The electric probe shown in the right is used for both of the E_x and E_z components at the proper orientation, and the electric probe shown in the left – for the E_y component. The probe for the E_x and E_z components inevitably contains a small vertical section that arises in some extent a registration of the E_y component, as well.

I. I. Arestova is with the Faculty of Physics, University of Sofia, Bulgaria (phone: 359-2-8161724; e-mail: ilar@phys.uni-sofia.bg).

V. P. Levcheva is with the Faculty of Physics, University of Sofia, Bulgaria (phone: 359-2-8161724; e-mail: levcheva@phys.uni-sofia.bg).
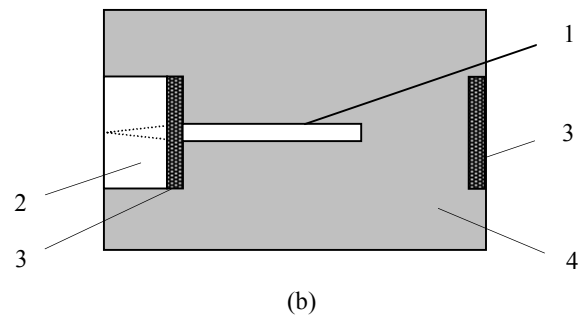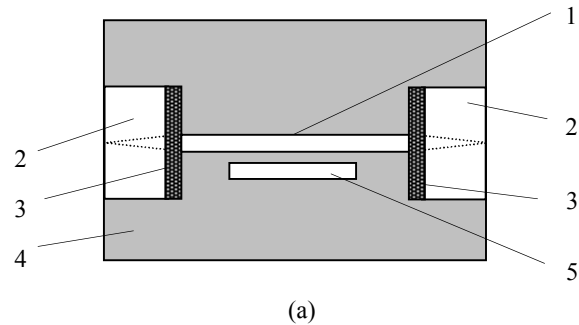
Fig. 1: The top views of the image guide structures.
(a) coupled IG structure; (b) single open ended IG.
1 − IG; 2 − rectangular waveguide to IG transition; 3 − absorbing plates; 4 − metal plate; 5 − secondary IG.
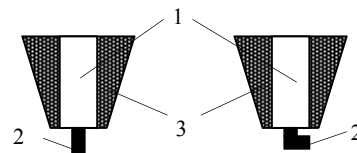
Fig. 2: The electric probes for E_y component (left) and E_x and E_z components (right).
1 – semi-rigid coaxial cable; 2 – inner conductor; 3 – absorbing coating.
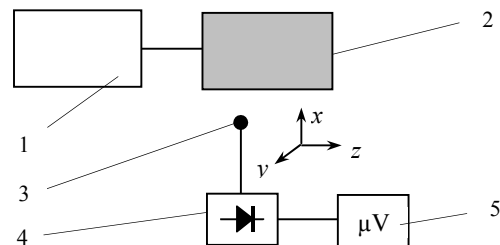
Fig. 3: The experimental setup.
1 – generator; 2 – the structure under investigation; 3 – the movable electric probe; 4 – detector; 5 – microvoltmeter.

(a)

(b)
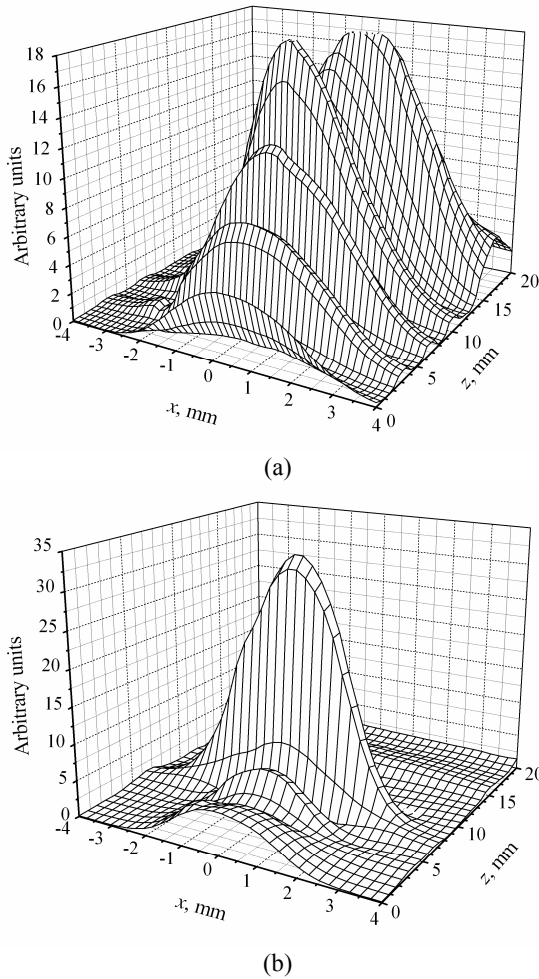
Fig. 4: The measured distributions of the E_x (a) and E_z (b) components.

The electric probe has been mounted on a three axes vernier mechanism that allows positioning the probe along these three axes. During all measurements the electric probes were kept on a height of 0.6 mm above the dielectric core. The experimental setup is shown in Fig. 3. The generator used works in a frequency range from 26 GHz to 38 GHz.

The measured distributions of the electric field components in an open ended IG section made from alumina ($\varepsilon_r = 9.6$, $tg\delta_\varepsilon = 1.10^{-4}$) with a length of 10 mm and a cross section of 1.80 mm x 0.97 mm are shown in Fig. 4. The quantity along the vertical axis, which is measured in arbitrary units, is proportional to the squared electric field components due to the square-law characteristic of the detector. The origin of the x-axis is at the middle of the dielectric core of the IG. The distribution of the E_y component is similar to that of the E_x component differentiated from it by its higher level.

The distributions of both E_x and E_z components have shown a strong increase from the input ($z = 0$) to the open end of the dielectric core ($z = 10$ mm). The main difference between the distributions of the E_x and E_z components is

that the E_x component increases gradually (Fig. 4a), while the E_z component's increment is more locally associated with the open end (Fig. 4b). It's worth pointing out, that relatively large values of the measured quantity at distances z > 10 mm have been observed in the distribution in Fig. 4a, while in the other distribution in Fig. 4b the values are small enough in the same region.

The distribution of the measured fields at the open ended structure shows that in the vicinity of the dielectric core's end there are large electric fields. These fields should be taken into account in the design procedure of the components. They seem to be essential not only for the operating mechanism of the coupled IG structures, but also from the point of view of the electromagnetic compatibility of such type of devices.

I. SIMULATION RESULTS

The simulated distribution of the electric field for the open ended structure which was made using a 3D electromagnetic simulator Ansoft HFSS [5], is shown in Fig. 5. The picture observed could be treated as a transformation of the bound mode in the IG to the radiated field.

The simulated results for the near field at a frequency of 33 GHz are presented in Fig. 6. The 2D polar diagrams of the electric field components for a distance $r = 10$ mm are shown in Fig. 6; the polar diagram in a horizontal plane ($\theta = 90°$) is presented in the Fig. 6a, and the one in the vertical plane ($\varphi = 90°$) – in the Fig. 6b. The distance $r = 10$ mm corresponds to the open end of the dielectric core of the IG. The diagram in the Fig. 6a shows that the E_z component has the greatest value among the other electric field components. This is in accordance with the measured distributions shown in Fig. 4. The diagram in the vertical plane (Fig. 6b) has a strong maximum at about $\theta = 0°$ for the E_y component and at about $\theta = 10°$ for the E_z component.

The polar diagrams of the electric field components for a distance $r = 20$ mm are shown in Fig. 6; the polar diagram in a horizontal plane ($\theta = 90°$) is presented in the Fig. 6c, and the one in the vertical plane ($\varphi = 90°$) – in the Fig. 6d. The distance $r = 20$ mm corresponds to the maximum z in the model used (Fig. 5). The E_z component continues to be the greatest electric field component in the horizontal plane (Fig. 6c) followed by the large enough E_y component, while the E_x component is relatively small. The diagram in the vertical plane (Fig. 6d) has been modified with an increment of the distance r – the maximum of the E_z component has moved to about $\theta = 30°$. The maximum of the E_y component continues to stay at about $\theta = 0°$.

The simulated 2D polar diagrams for the far field at a frequency of 33 GHz are shown in Fig. 7. The polar diagram in the horizontal plane ($\theta = 90°$) is presented in Fig. 7a, and the one in the vertical plane ($\varphi = 90°$) – in Fig. 7b. The main lobe of the radiated field in the horizontal plane has a maximum at $\varphi = 0°$. The
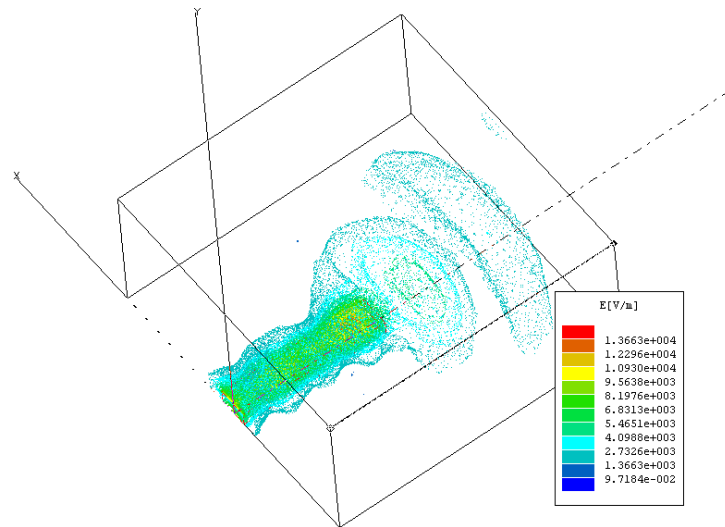
Fig. 5: Simulated distribution of the magnitude of the electric field at 33 GHz.

(a)

(b)

(c)

(d)
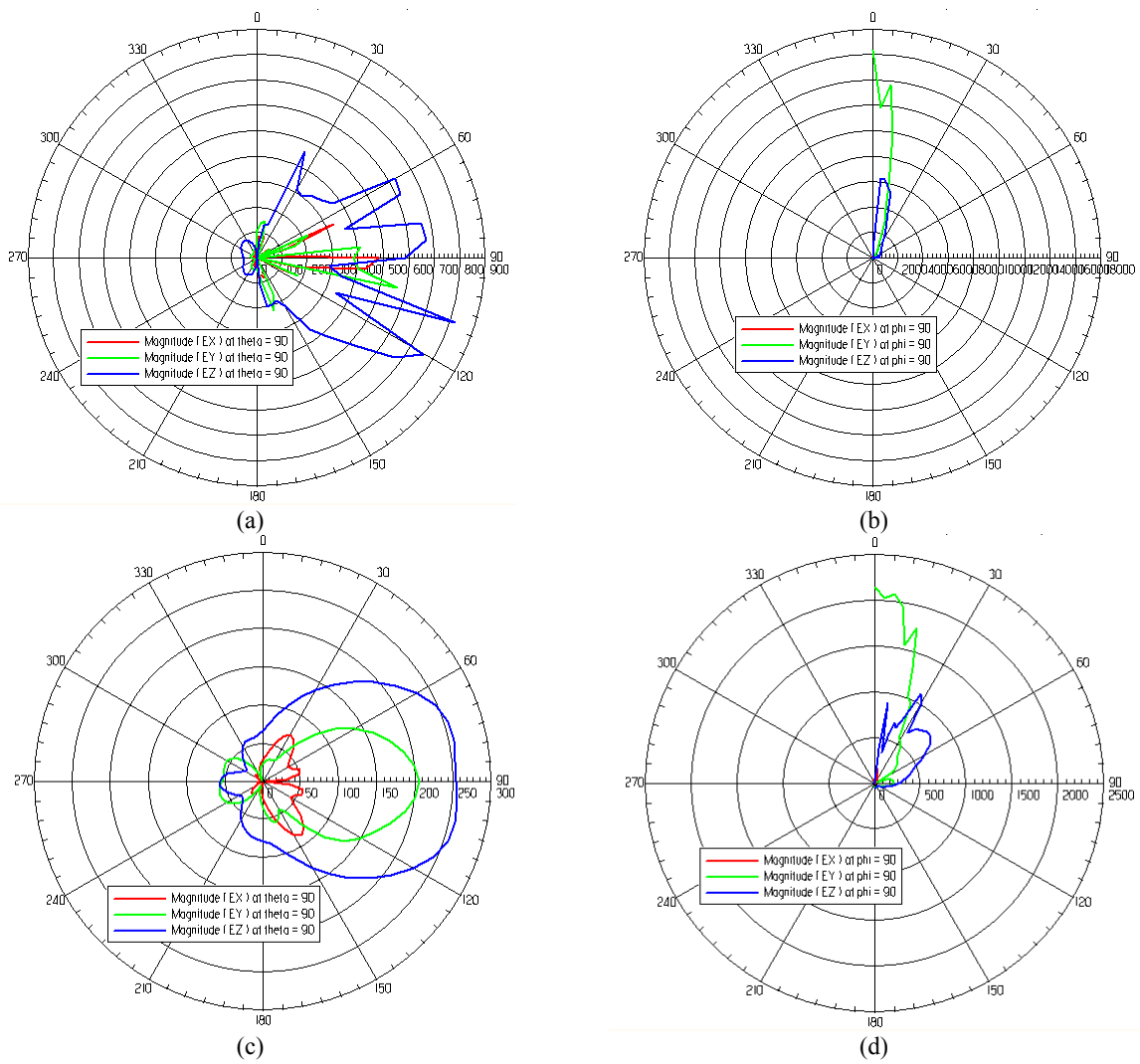
Fig. 6: Simulated polar diagrams for the near field at a frequency 33 GHz.
(a) r = 10 mm, θ = 90º; (b) r = 10 mm, φ = 90º;
(a) r = 20 mm, θ = 90º; (b) r = 20 mm, φ = 90º.

(a)   (b)
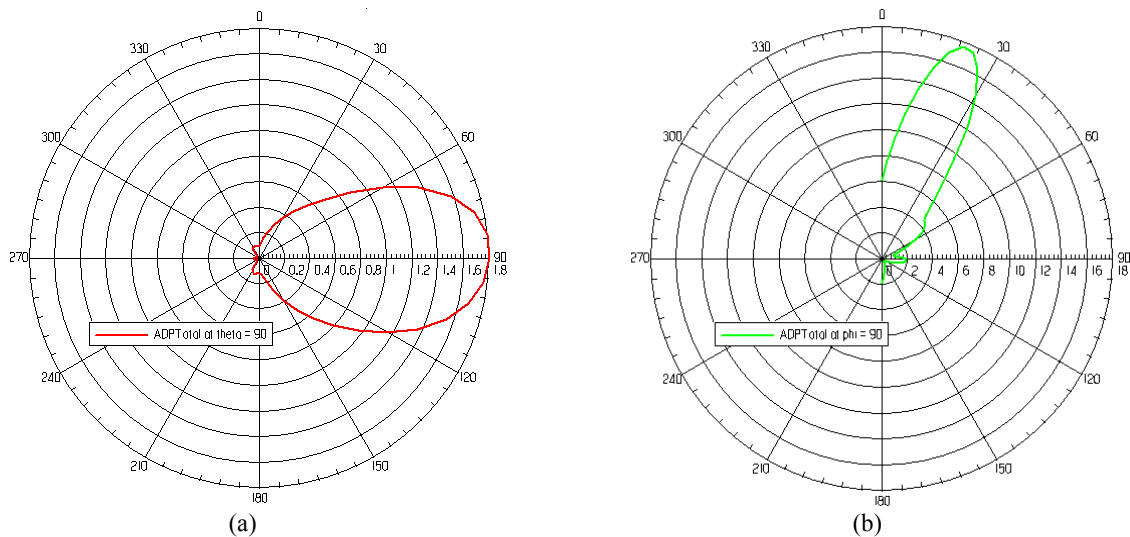
Fig. 7: Simulated polar diagrams for the far field at a frequency 33 GHz.
(a) $\theta = 90º$; (b) $\varphi = 90º$.
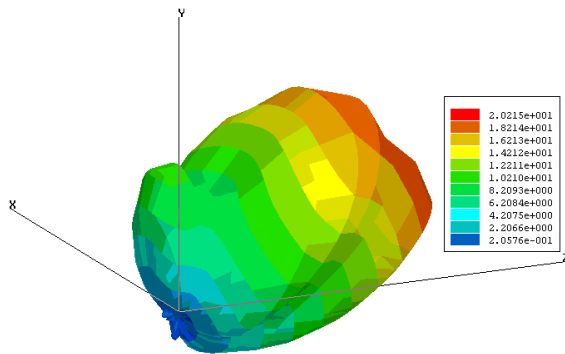
Fig. 8: Simulated 3D antenna directivity pattern at 33 GHz.

beamwidth is equal to about 70º and there are small backlobes too. The main lobe of the radiated field in the vertical plane has a maximum at about $\varphi = 22º$ and its beamwidth is equal to about 30º.

The simulated 3D antenna directivity pattern at 33 GHz is shown in Fig. 8 as an illustration. This potato-shaped diagram is tilted at an angle of about 30º with respect to the z axis and has a considerable beamwidth in both horizontal and vertical planes.

IV. CONCLUSION

The experimental and numerical investigation performed has shown the significance of the processes of radiation at the open end of the IG. The next step could be the numerical investigation of the radiation effects in the couple IG structure.

REFERENCES

[1] S. J. Fiedziuszko, I. C. Hunter, T. Itoh, Y. Kobayashi, T. Nishikawa, S. N. Stitzer and K. Wakino, "Dielectric materials, devices and circuits", *IEEE Trans. Microwave Theory Tech.*, vol. 50, pp. 706 – 720, March 2002.

[2] Wolfgang Menzel. 2008 August. 50 years of millimeter-waves: A journey of development. *Microwave Journal*. Vol. 51. Available: http://www.mwjournal.com

[3] Iliyana I. Arestova, Plamen I. Dankov and Valda P. Levcheva, "A study on the coupled image guide structures", in *PIERS (Progress In Electromagnetics Research Symposium) Proceedings*, Moscow, 2009, 1204-1209.

[4] I. I. Arestova and S. A. Ivanov, "Nonreciprocal effects in coupled ferrite-dielectric image guide structures", in *XII ICMF (International Conference on Microwave Ferrites) Proceedings*, Gyulechica, Bulgaria, 1994, 188-192.

[5] *Ansoft HFSS User's Manual* , A Full-Wave Spice Problem, 2001.